Optimized Sliding Mode Regulation based on Particle Swarm Optimization Algorithm for Non-linear DFIG-Wind Turbine

Omar Busati Alzain[1], **Xiangjie Liu**[2], **Xiaobing Kong**[3]

[1,2,3] *School of Control and Computer Engineering, North China Electric Power University,Beijing,102206, China (e-mail: omarbusati@ncepu.edu.cn;omarbusati@gmail.com).*
[1] *Department of Electronic and Electrical Engineering, Faculty of Engineering, International University of Africa, Khartoum, Sudan*

Abstract: The inherent growth of the non-linear effects, wind-speed swings, and parameters uncertainty are challenges in the modern power system based on wind turbines, including a doubly fed induction generator (DFIG-WT). In addition to being subject to voltage drop conditions, it is necessary to design reliable control units to meet the system's nominal power. According to these considerations, a new rotor-aspect current control that revolves on active- and reactive-power (Ps-Qs) control is suggested using a sliding mode technique via discrete particle swarm optimization control (RPSMC-PSO) based on the recurrent construction of neural network (RNN) for the non-linear DFIG-WT. Based on features of the low-degree Taylor approximation principle, the RNN is re-constructed to simplify the optimization problem of the PSO to generate the optimal sliding switch signals. The main idea of this routine is to force the quasi-chatter behavior of SMC for the non-linear system to be close to the optimal sliding trajectory in a few steps and less calculation burden of the algorithm. Thus, the control law guarantees the general stability of the system and attenuates the unimportant chatter impacts. Also, the suggested control approach is compared against the standard control as SMC and Proportional-Integral regulator (PI). Moreover, a 1.5 MW DFIG is inspected to validate the dynamic results of the open-source FAST turbine model. Dynamic results show preference of RPSMC-PSO in terms of dynamic changes of the DFIG-WT under numerous experimental achievements comparing with the standard control approaches.

Keywords: DFIG, sliding mode control, harmonic distortion, power system control, wind power generation.

1. INTRODUCTION

Given the speed increase in the greenhouse gas emissions resulting from the expansion of industrial activities that use fossil fuels, many countries have turned to alternative energy for reducing the degradation of the Earth's environmental cover. In this context, wind generation systems represent a promising and cheaper alternative and can provide enough energy that contributes to solving global energy challenges (Valenciaga and Puleston, 2008; Qiao et al., 2009). The power grids system current design based on the wind turbine (WT) uses a doubly-fed induction generator (DFIG) due to having many advantages compared with the synchronous generators. These advantages are summarized in that: it has four-quadrant power regions with a low transformation rate of energy, a wide array of altered speeds, and the ability to enhance the regulation techniques that reduce equipment cost and dynamic losses (Ganti et al., 2011; Pande et al., 2013; Nazari et al., 2011). Moreover, the dips and disturbances effects, non-linear behavior, and the complexity of the DFIG-WTs need to design effective and robust regulators to increase the total efficiency. For that, the standard regulator, such as the Proportional-Integral regulator (PI), fails to find a precise solution for stability problems. Consequently, various intelligent regulation approaches have been indicated in many studies for improving system performance. Experimentally, robust control in the stationary $\alpha\beta$ reference frame has guaranteed stable regulation of DFIG-WTs under (normal/dips) of grid voltage, and disturbances condition with emerged chattering can deteriorate the dynamic variables, especially in the case of the first detection of the fault (Costa et al., 2010). In (Jabr et al., 2011), the stator-aspect power control-based Neuro-Fuzzy (NFC) needs collective experiments data to include all different dynamic test conditions associated with the standard PI controller. The adapted PI coefficients based on NFC are extracted at *dq*-reference level related to the rotor-aspect voltage from the scheduled vector applied on DFIG-WT. Further analysis at dq-level for the stator- and grid-aspect control components connection based on PI controller with separation units and a rotor-aspect current controller plus the resonant units have been offered in (Zhou et al., 2009; Xu et al., 2012). These reference-level analyses of DFIG-

WT have enhanced the design of the proposed regulator in the current topic.

Sliding-Mode regulation formula (SMC) has been successfully used to manipulate some control issues in practical applications due to its unmentioned sensitivity to external disturbances and unwanted dynamic changes for DFIG and WTs in (Beltran et al., 2008; Young et al., 1999; Hu et al., 2010a; Martinez et al., 2013). However, the impact of sliding chatter (SCE) is a frequent challenge in SMC, besides meeting the regulation aims for many applications aspects due to the classical design of sliding switches term based on saturation restrictions that may emerge excessive chattering in the system. The classical design of sliding switching was introduced in many aspects of DFIG-WT, such as the direct SMC regulation of DFIG through extended active power under normal and dips voltage conditions in $\alpha\beta$-level (Sun et al., 2017), the back-stepping-based adaptive-SMC control has offered accurate regulation aims for the stator-aspect power of multi-generator energy networks based on DFIG in (Patnaik and Dash, 2016). Separately in (Martinez et al., 2012; Chen et al., 2009), Integral-SMC based on classical sliding chatter saturation law has been offered based on direct stator-aspect reactive power, and As well, the torque regulation at dq- reference level during dips and harmonic effects on the grid voltage. Regulation of the direct stator-aspect power that involves Integral-SMC plus 2-times actual frequency compensator has been achieved for the DFIG system during the imbalanced condition (Shang and Hu, 2012). SMC based on classical sliding switching law in the $\alpha\beta$-level for the stator-aspect power control toward the rotor-aspect plus compensation unit during unbalanced DFIG was designed in (Sun and Wang, 2017). Generally, the common sliding chattering control term based on sliding variables, boundaries, and signs was used in earlier SMC studies, which causes an unsteady slide for system sequences states on the effective surface to meet the dynamic characteristics. Avoiding the arithmetic burden, consumed time, search for the optimization regions, and meeting the regulation objectives are inevitable challenges when using predictive and heuristic algorithms for many application fields. Many solutions in Model Predictive Controller (MPC) have been introduced related to the DFIG-WT, such as a high sampling-time and avoid inspecting whole executable voltage arrays in (Cheng and Nian, 2017; Zhang and Hou, 2017), respectively. As well as, in(Liu and Kong, 2013), the first-step prediction sequence feature-based non-linear MPC was presented for controlling the DFIG-WTs under abnormal conditions. These features with the standard augmented formula are used in this proposed study to build a first-order sliding vector based on rotor-aspect current.

The accurate design of advanced regulation approaches depends on accurate actual paradigms in continuous- and discrete-domain cases. Therefore, several common modeling techniques are designed from collected processing dataset, such as mining approach, forward-neural networks (FFNNs) and recurrent neural networks (RNNs) (Repta et al., 2018; Pan and Wang, 2011; Akpan and Hassapis, 2011), respectively. This study builds the RNNs paradigm in the light of previous studies with some necessary modifications to find the linear paradigm as mentioned in the next paragraph and subsection 2.2. From the standpoint of modeling, RNNs are highly competitive with non-linear dynamic behavior and, FFNNs are more convenient in static function (Zamarreño and Vega, 1998). The MPC based on RNN is essentially depending on the accurately training procedures and their system-based data. Thus, the predictive neural paradigm will offer unstable behavior when it exceeds the range of training information for the non-linear system (Guo et al., 2014; Qin and Badgwell, 2003). According to these reasons, the Taylor series formula has been accurately offered based on enhanced RNNs for designing a linear predictive control (Xiang et al., 2016).

More optimization approaches based on heuristic ways have been presented to obtain an approximate (nevertheless, not inevitably the best) solution. These methods accelerate searching for optimal points and enable the combination of various random adjustment methods. The standard solutions of these methods contain evolutionary and swarm algorithms, such as Genetic, Particle Swarm (PSO), BAT, Bird Swarm algorithm, etc. Optimization approaches based on the traditional adaptation such as the computation formula, offline-PSO, and offline-BAT algorithm have an essential shortage involving ideal modeling of the system with off-line iteration without computed the unknown dynamic changes (Ruiz-Cruz et al., 2012; Yılmaz and Küçüksille, 2015). Thus, the system may lead to a decrease the overall efficiency. Nature-inspired algorithms have been introduced in many aspects of distorted DFIG-WT. (Alzain et al., 2019) displayed a rotor-aspect current control based on the online tuned PI-resonant regulator using BAT Algorithm (PIR-BAT) for the linear paradigm of 2 MW-DFIG-based WT. PIR-BAT handled the dynamic signal at a primary frequency and 5th and 7th-order of harmonic without additional calculation in the sequences of harmonic spectrum items on the rotor-aspect current. PIR-BAT mechanism presented lower search burdens with 6e−4 MSE over 10 iterations and satisfactory dynamic reactions compared to ordinary regulators. Besides, (Alzain et al., 2021) presented a rotor-aspect current control based on the online tuned SMC-Resonant regulator using Bird Swarm Algorithm (SMCR-ABSA) based on the linear model of 2 MW-DFIG. SMCR-ABSA suppressed the emerged ripples of 5th- and 7th-order harmonic and regulated the main dynamic signal without extra calculation in the sequences of harmonic items on the rotor-aspect current. SMCR-ABSA mechanism offered a lower convergence burden over 60 iterations and better dynamic reactions compared to common regulators. A dq-rotor-aspect current control based on predicted SMC using BAT Algorithm (BATS-SMC) for the linear paradigm of the 1.5 MW DFIG-WT has been presented in (Omar et al., 2021). BATS-SMC mechanism dealt with a fixed rotor-speed scenario to introduce a lower search burden with 5.8e−4 MSE along 10 iterations and satisfactory dynamic reactions compared to common regulators.

Furthermore, Slime Mould (SMA) algorithm is one of the metaheuristic methods that provided a higher achievement and fewer computations time for finding the ideal adapted coefficients of PI-Fuzzy regulator associated with the servo applications. SMA optimization target is specified as the multiplication of sum of time and squared system error

(Precup et al., 2021). This proposed topic introduced the PSO algorithm, a random directive algorithm (Zeddini et al., 2016). PSO produces random particles in the searching range and looks for the best choice among the population of swarm solutions. Then, an individual particle, location, and speed are defined at a sample interval to determine the best convergence (Rekioua, 2014). In addition, the merged PSO with standard algorithms and controllers in various researches has accomplished substantial positive dynamic reactions within the improvement of the regulation fields. The hybrid algorithm, especially in the swarm system, is necessary to reduce detected deficiencies while using standard algorithms. These hybrid swarm algorithms could have a higher ability to reduce detected optimization problems while using standard algorithms. Also, PSO's trade-off between observation and manipulation features has been applied in 3D construction to improve the convergence and iterations of the self-assembly computation approach (SAPSO) based on the Euclidean optimization target, which is specified as the distance term between the agents-elements and construction elements (Zapata et al., 2020).

This proposed topic considers that dealing with the chattering behavior of the sliding plane is essential to guarantee system stability. Therefore, SMC investigations have been implemented while reducing the chattering effects during several operation cases of the DFIG-WTs by merging the features of SMC, RNN, and PSO algorithms. The RNN based on non-linear DFIG has been simplified by rebuilding it as the low order of the Taylor approximation equation for system-based control representation (Balduzzi et al., 2017). Taylor-based RNN is used for applying the sequences of state-space on the PSO optimization strategy. Thus, the optimal correction of the sliding chattering sequences is performed at each sample time to minimize the optimization function of the sliding sequences as the main contribution of design. The optimization function is defined as the sum of squared error of sliding states based on rotor-aspect current and the predicted control signal sequences based on the PSO algorithm. In addition, the PSO algorithm generates the predicted control law solutions of SMC and the identical control law to ensure the accuracy of the state path of the sliding switches during the future sampling time without chattering behavior. According to the structure of RPSMC-PSO control, the controller is divided into conventional SMC model control plus predicted sliding terms to correct the sequences of non-linear behavior as perturbations (Xu and Li, 2011). These features perfectly regulated the non-linear behavior in DFIG, abrupt modification in current, torque, and related quantities. In general, this topic presents a rotor-aspect current control mechanism based on active and reactive power using an optimal sliding mode control approach RPSMC-PSO. The suggested mechanism and traditional control are applied to the rotor- and grid-aspect bi-way IGBT converters. The low-order Taylor approximation formula of the RNN frame is applied to the grid-connected DFIG-WT. RPSMC-PSO unit included a PSO algorithm based on the RNN, which uses the MIMO variables of the system to detect optimum sliding chattering trajectories. Thus, RPSMC-PSO delivered the dq-axis rotor voltage as control signals to the rotor-aspect converter.

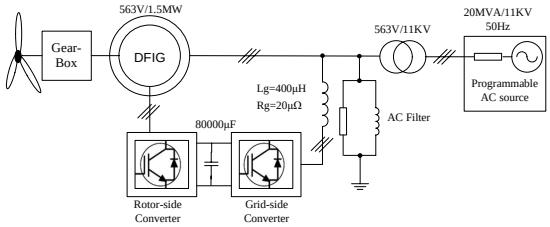

Fig. 1. The public diagram of DFIG-WTS.

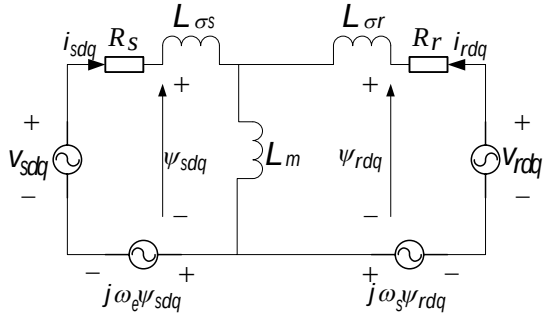

Fig. 2. DFIG ideal-circuit at dq-reference mode.

2. SYSTEM DESCRIPTION

2.1 Description of the DFIG model

WT system converts the energy of wind movement into useful electric energy through the non-linear relationships between the components of the mechanical and electrical units. In the modern WTs that general connections are represented in Fig. 1, DFIG is generally an essential and common element in the building of the WTs due to its dynamic outperforms compared with the synchronous generators. As well as one of its striking features, it has design flexibility that allows the development of control system units to obtain a continuous and stable energy supply. In general, the vector control method uses the reference frames approach to simplify the DFIGs variables according to the rotation at angular speed. In this study, the mathematical relationships of the DFIG can be derived assuming that: all parameters and variables are scaled using Per/Unit criteria; the model is analyzed in an arbitrary reference frame (dq) in which the rotational speed is close to the angular speed of the generator ω_e and the simple circuit of the DFIG has a symmetrical air-gap (Liu and Kong, 2013; Hu et al., 2010b). Referring to the simple equivalent circuit Fig. 2, the voltage compact form based on dq-frame can be expressed as:

$$\begin{aligned} v_{sdq} &= R_s i_{sdq} + \frac{d\psi_{sdq}}{dt} + j\omega_e \psi_{sdq} \\ v_{sdq} &= R_r i_{rdq} + \frac{d\psi_{rdq}}{dt} + j\left(\omega_e - \omega_r\right)\psi_{rdq} \end{aligned} \tag{1}$$

and

$$\begin{aligned} \psi_{sdq} &= L_s i_{sdq} + L_m i_{rdq} \\ \psi_{rdq} &= L_m i_{sdq} + L_r i_{rdq} \\ L_s &= L_{\sigma s} + L_m \\ L_r &= L_{\sigma r} + L_m \end{aligned} \tag{2}$$

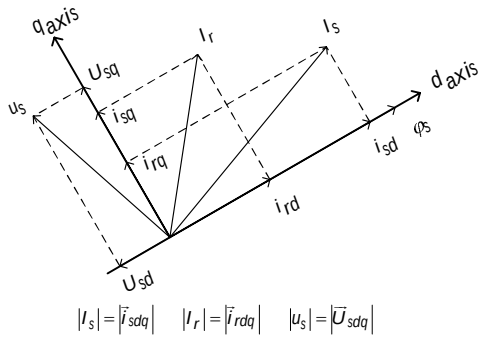

Fig. 3. The scheme of oriented phasor for the stator flux.

where $v_{sdq}, v_{sdq}, i_{sdq}, i_{rdq}, \psi_{sdq}$ and ψ_{rdq} are the dq-axis vectors of voltages, currents and fluxes of the stator-aspect and rotor-aspect, respectively. $R_s, R_r, L_s, L_r, L_{\sigma s}, L_{\sigma r}$ and L_m are the resistances, winding interior self-inductance and leakage inductance of stator-aspect and rotor-aspect, respectively. The linear model of DFIG can be specified relating to u_s and ψ_s as constant amounts, and the stationary resistive voltage drop is removed. Therefore, $v_{sd} = 0$ and $v_{sq} = U_s$, and by including (2), the equation (1) is written as:

$$\begin{aligned} v_{sdq} &= R_s i_{sdq} + j\omega_e \psi_{sdq} \\ v_{sdq} &= R_r i_{rdq} + (L_{sm} - \frac{L_r L_s}{L_m})\frac{di_{sdq}}{dt} + j\,(\omega_e - \omega_r)\,\psi_{rdq} \end{aligned} \tag{3}$$

In (Shi et al., 2019), the non-linear model of a DFIG under varying circumstances of the grid can be specified with merging and rewriting (1), (2) and (3), and the fluxes stator-aspect are taken in computations. With indicating to the stator-aspect flux orientation (SFO) phase diagram Fig. 3, the direct axis of reference scheme arrayed with the stator-aspect flux. Hence, $\psi_{sd} = \psi_s$ and $\psi_{sq} = 0$. The non-linear DFIG formula can be expressed as a function of i_{sdq} and i_{rdq}

$$\begin{aligned} di_{sd}/dt &= \mathrm{H}_1 i_{sd} + \mathrm{H}_2 i_{sq} + \mathrm{H}_3 i_{rd} + \mathrm{H}_4 i_{rq} + \mathrm{N}_1 v_{sd} + \mathrm{N}_2 v_{rd} \\ di_{sq}/dt &= \mathrm{H}_5 i_{sd} + \mathrm{H}_6 i_{sq} + \mathrm{H}_7 i_{rd} + \mathrm{H}_8 i_{rq} + \mathrm{N}_1 v_{sq} + \mathrm{N}_2 v_{rq} \\ di_{rd}/dt &= \mathrm{G}_1 i_{sd} + \mathrm{G}_2 i_{sq} + \mathrm{G}_3 i_{rd} + \mathrm{G}_4 i_{rq} + \mathrm{M}_1 v_{sd} + \mathrm{M}_2 v_{rd} \\ di_{rq}/dt &= \mathrm{G}_5 i_{sd} + \mathrm{G}_6 i_{sq} + \mathrm{G}_7 i_{rd} + \mathrm{G}_8 i_{rq} + \mathrm{M}_1 v_{sq} + \mathrm{M}_2 v_{rq} \\ d\omega_s/dt &= PL_m/J\,(i_{sq} i_{rd} - i_{sd} i_{rq}) - T_m/J \end{aligned} \tag{4}$$

where

$$\begin{aligned} \mathrm{H}_{1,6} &= -R_s/L_s\sigma, & \mathrm{H}_{2,5} &= \pm\sigma^{-1}\frac{\omega_e - \omega_s L_m^2}{L_s L_r} \\ \mathrm{H}_{3,8} &= \frac{R_r L_m - L_r L_m}{L_s L_r - L_m^2}, & \mathrm{H}_{4,7} &= \mp\frac{\omega_s L_m}{L_s\sigma} \\ \mathrm{G}_{1,6} &= -R_s L_m/L_s L_r\sigma, & \mathrm{G}_{2,5} &= \mp(\omega_e - \omega_s)L_m/L_r\sigma \\ \mathrm{G}_{3,8} &= -\frac{R_r L_s - L_m^2}{L_s L_r - L_m^2}, & \mathrm{G}_{4,7} &= \pm\omega_s/\sigma \\ \mathrm{N}_1 &= 1/L_s\sigma, & \mathrm{N}_2 &= L_m/L_s L_r - L_m^2 \\ \mathrm{M}_1 &= -L_m/L_s L_r\sigma, & \mathrm{M}_2 &= -L_m^2/L_s L_r^2\sigma \\ \sigma &= 1 - L_m^2/L_s L_r. \end{aligned}$$

The first-degree differential of stationary angular speed depends on the shaft rotor-aspect angular speed, which can be formed by involving the electromagnetic torque T_e, the wind turbine torque T_m and the moment of inertia J:

$$\begin{aligned} T_e &= 3pL_m.\,\mathrm{Im}\{\underline{I}_r.\underline{I}_s\} \\ J\frac{d\omega}{dt} &= T_m - T_e \end{aligned} \tag{5}$$

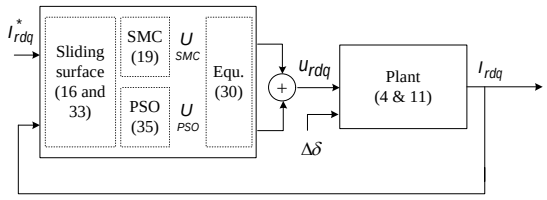

Fig. 4. RPSMC-PSO approach model of rotor-aspect current control.

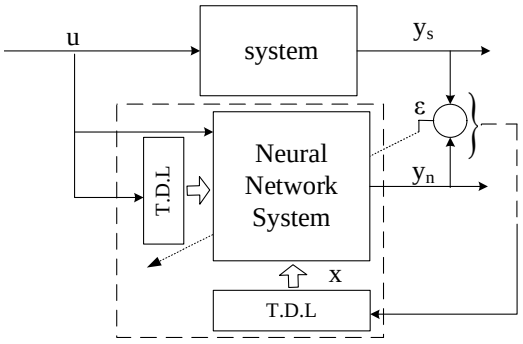

Fig. 5. Two paradigms of learning approaches are defined as non-linear parallel-/series–parallel type.

where $T_m = 0.5\rho\pi R^3 C_\rho\,(\lambda, \beta)\,v^2$ with a radius and power coefficient of the rotor, wind speed, tip-speed rate and blade changes as R, C_ρ, v, λ and β respectively. The stator-aspect power Ps and Qs can be represented as

$$\begin{pmatrix} P \\ Q \end{pmatrix} = \begin{pmatrix} \mathrm{Re}\{\underline{V}_s.\underline{I}_s\} \\ \mathrm{Im}\{\underline{V}_s.\underline{I}_s\} \end{pmatrix} \tag{6}$$

2.2 Suggested Control Modelling

The overall structure of rotor-aspect control using RPSMC-PSO based on RNN structure is shown in Fig. 4. Also, the general types of FNN-NARX (non-linear Auto-regression eXogenous architecture) based RNN structure are shown in Fig. 5. According to the position of neural units within the system construction, two common training approaches are generated to evaluate the weight gains of the neural model. In this investigation, the first approach called the non-linear parallel model is used, with the previously evaluated output signals are defined as feedback into the neural system through the tapped delay line (TDL). The non-linear series-parallel model can be designed as a second approach, with the real paradigm output is linked with the neural system through TDL (Wang et al., 2015; Zemouri et al., 2010).

$$\begin{pmatrix} P \\ Q \end{pmatrix} \overset{def}{=} -3/2 \begin{pmatrix} u_s i_{sq} \\ u_s i_{sd} \end{pmatrix} \tag{7}$$

In (Balduzzi et al., 2017), the sequences of input/output behavior for the model dynamics (4) can be built as the NRAX for the RNN. This kind of RNN utilizes retrogression elements φ to find the estimated future output based on a non-affine form f_a as:

$$\bar{y}_{k+1} = f_a(\varphi_k, \varepsilon) \tag{8}$$

Referring to the formula (4) and (7), the vector of retrogression variables is defined as, $\varphi_k = [x_{k+r-1}, ..., x_{k+r-m_y},$

$u_k, ..., u_{k-m_u+1}]$. where my and mu are +fixed scalar index to determine the retrogression vector extension as (my, mu) corresponding to the past delayed values of output x and input signals u. The label ε in (8) is a pure additive white un-rated noise that accompanies a series of input and output estimates. An accurate equivalent model is complicated to be built for a real MIMO system. Therefore, this paper identifies the MIMO real system as two MISO subsystem neural network models to be an alternative to a single MIMO form of the entire process as in (Yu and Gomm, 2003), as well, the MISO sub-system neural network is collected from a compound of two feed-forward neural networks. Then, the MIMO equivalent structure can be built using correctly coupling MISO models. Thus, the new retrogression vector of NARX model can be defined by an interior regression vector and input signals as $\varphi_k = [\varphi'_k, u_k]$. where $\varphi'_k = [x_{k+r-1}, ..., x_{k+r-m_y}, u_{k-1}, ..., u_{k-m_u+1}]$ is the inner RNN retrogression vector to result the affine discrete-time of input/output prediction form as

$$\begin{aligned} \varphi'_{k+1} &= f(\varphi'_k) + g(\varphi'_k).u_k + \bar{\omega} \\ y_k &= h(\varphi'_k) \end{aligned} \tag{9}$$

where f and g are identified as the feed-forward neural networks with two manipulated inputs, each one has single output and multi-inputs. By the Taylor series formula applied to recurrent neural network architecture in (Yan and Wang, 2012), the dynamic variables of the model are defined to be quantifiable. The RNN is re-formed using a low degree of Taylor structure around the operating values ($[\varphi'_0(k)]$) that are determined as previous successions of input/output. Thus, the non-linear part is decomposed into a new affine structure for the entire time interval.

$$\begin{aligned} \varphi'(k+1) &= f_{fg}(\varphi'_0(k)) + \left(\frac{\partial f_{fg}(\varphi')}{\partial x}\Big|_{\varphi'_0(k)} \right)(x - x_0) \\ &+ \left(\frac{\partial g(\varphi')}{\partial u}\Big|_{\varphi'_0(k)} \right)(u - u_0) + \bar{\omega} \\ &= \Delta x_{k+1} = A(x - x_0) + B(u - u_0) + \bar{\delta}_k \\ y(k) &= h(\varphi'_0(k)) + \left(\frac{\partial h(\varphi')}{\partial x}\Big|_{\varphi'_0(k)} \right)(x - x_0) \\ &= \Delta y_k = C(x - x_0) \end{aligned} \tag{10}$$

The associated state variables are approximated pursuant to: the constant terms of (10) are equal to the state and output initial point. The constant matrices of the state variables, input and output are identified as $A = \frac{\partial f_{fg}}{\partial x}\Big|_{\varphi'_0}$, $B = \frac{\partial g}{\partial u}\Big|_{\varphi'_0}$ and $C = \frac{\partial h}{\partial x}\Big|_{\varphi'_0}$ respectively. Generally, the model in (4) is shaped as a linear relationship (10) including low-order Taylor chains through the particular operation points for the sigmoid-elements of each destination node. The stable state model of the system can be expressed in the general formula as:

$$\begin{aligned} \Delta x_{k+1} &= \mathrm{A}\Delta x_k + \mathrm{B}\Delta u_k + \bar{\delta}_k \\ \Delta y_k &= \mathrm{C}\Delta x_k \end{aligned} \tag{11}$$

A three-stage delay model for the RNN related to the DFIG model having named gains was assumed in the simulation results section. This design is achieved using I/O data are obtained from the FAST open design WT model in Matlab software to verify the RNN during tuning weight gains condition. FAST-platform is offered by American National Renewable Energy Laboratory (NREL) as in Fig. 6. The series of input data without noise was created randomly to generate output responses along 200 samples as represented in Fig. 7. Each RNN is assembled from two feed-forward neural networks f and g and has two inputs and one output. Each net has eight input sequences and three output feedback sequences through TDL units. The number of *f,g*-networks hidden sigmoid nodes are set as [5 and 3], and the linear output nodes are set as [1 and 1], respectively. The training algorithm uses gradient back-propagation for achieving the learning. The training performance scheme in Fig. 8 (a) shows the relationship of the Mean Squared Error (MSE) for the train, validation, and test procedures along with the iterations, with the validation best points, are $4.114e-5$ and $1.5e-4$ at 15 epochs for trained *Irdq* model. The regression function between the output elements and related targets has been handled with 995 data samples for providing a higher precision about R=0.99961 and R=0.99408 for the two trained RNNs related to *dq* rotor-aspect current model respectively in Fig. 8 (b).

2.3 Discrete-Time Sliding Model Control Formula

Several studies have developed the discrete time-SMC control, including the model, for selecting the appropriate sliding path based on proportional or integral law (Du et al., 2016; Su et al., 2016; Yu and Long, 2015), which was found by using quantities of the dynamic system or by predetermining the sliding path:

$$\Delta e_k = \Delta x_k - \Delta x_k^{ref} \tag{12}$$

The current paper assumes that the PI relationship as a sliding switch law to find optimal response under the unbalanced system voltage, where the dynamic state deviation is set as follows:

$$\Delta s_{k+1} = k_P \Delta e_{k+1} + k_I.\Delta \xi_{k+1} \tag{13}$$

where the array of the sliding chatters is described as $s = \{s_k | s_k = 0,\ k = 0, 1, ...\}$, and the shifted integration error is specified as

$$\Delta \xi_k = \Delta e_k + \Delta \xi_{k-1} \tag{14}$$

From equations (11) and (12)

$$\begin{aligned} \Delta e_{k+1} &= \Delta x_{k+1} - \Delta x_{k+1}^{ref} \\ &= A\Delta e_k + B\Delta u_k + \bar{\delta}_k - \Delta x_{k+1}^{ref} + A\Delta x_k^{ref} \\ &= A\Delta e_k + B\Delta u_k + d_k,\ d_k = \bar{\delta}_k - \Delta x_{k+1}^{ref} + A\Delta x_k^{ref} \end{aligned} \tag{15}$$

The related control signal Uc is considered to be the solution series of $\Delta s = s_{k+1} - s_k = 0$, s-element can be estimated as (Xu and Li, 2011).

$$\begin{aligned} \Delta s_k &= k_P e_{k+1} + k_I (e_{k+1} + \xi_k) \\ &= (k_P + k_I) \Delta e_{k+1} + k_I \Delta \xi_k \\ &= Ga\Delta e_{k+1} + k_I \Delta \xi_k \end{aligned} \tag{16}$$

Replacing (16) into (15) for estimating the sliding element

$$\Delta s_k = Ga\,(A\Delta e_k + B\Delta u_k + d_k) + k_I \Delta \xi_k \tag{17}$$

The applied control signal involves step-shift delay disturbance, can be specified as:

$$Uc_k = -(GaB)^{-1}(-\Delta s_k + GaA\Delta e_k + Gad_{k-1} + k_I \Delta \xi_k) \tag{18}$$

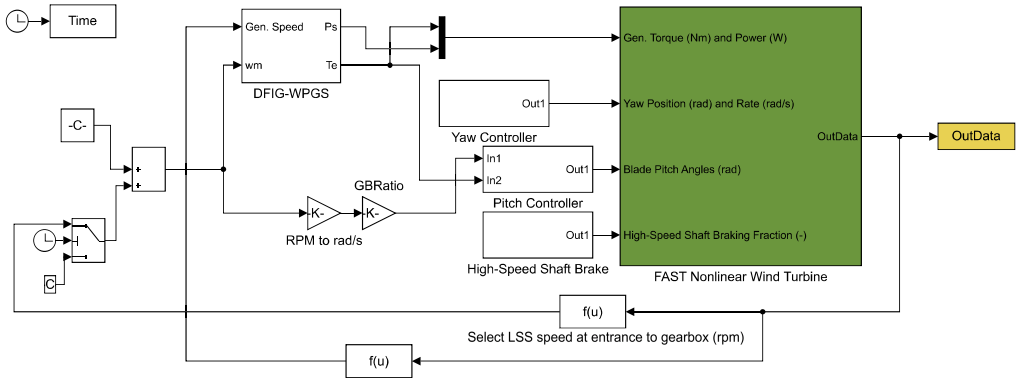

Fig. 6. FAST-based WT system

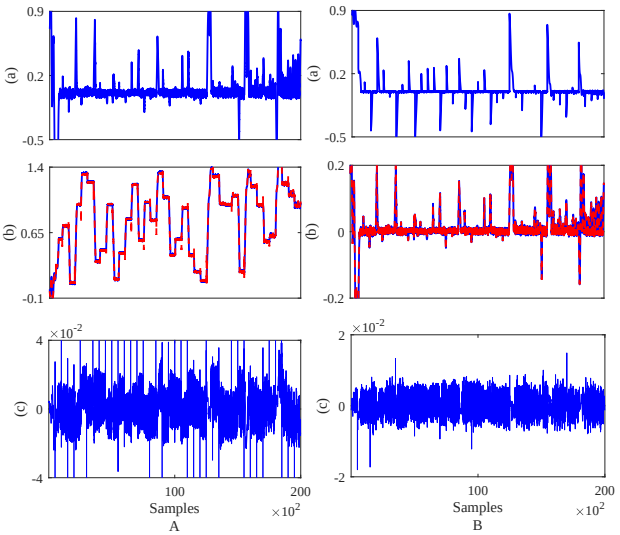

Fig. 7. Training steps for RNN (a) random signal for an input data, (b) validation of RNN for + dq-stator current (blue-plant) and (red-trained data), and (c) training errors. (A) + d-axis. (B) + q-axis.

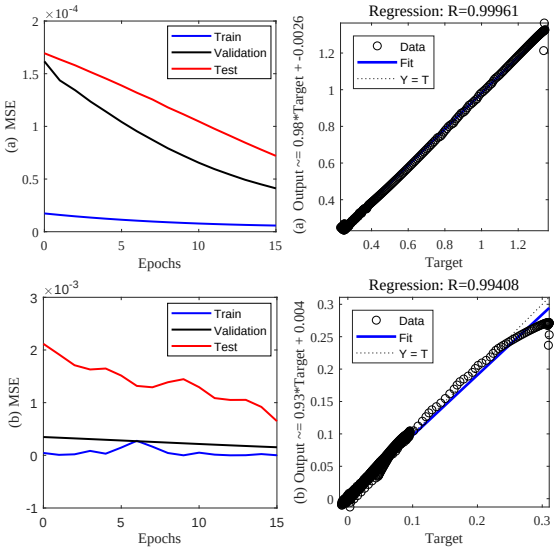

Fig. 8. Training and regression performance of the RNN for (a) d-axis of rotor-aspect current (b) q-axis of rotor-aspect current.

Define the difference of sliding mode as $s_{k+1} = s_k = 0$. Thus,

$$Uc_k = -(GaB)^{-1}(GaA\Delta e_k + Gad_{k-1} + k_I\Delta\xi_k) \quad (19)$$

One of the techniques that is regularly used is to extend the active control range with a separate swing term within the control signal $Usw_k = \mathrm{K}_m sign(s) + \eta s$, to compel the model state to realize sliding properties, and therefore, the overall control formula is defined as

$$U_k = Uc_k + Usw_k \quad (20)$$

Border layers are specified to reduce the chattering states as follows

$$\begin{cases} 1, & s > \underset{\sim}{\Delta} \\ \mathrm{ks}, & |s| \le \underset{\sim}{\Delta}, k = 1/\underset{\sim}{\Delta} \\ -1 & s < -\underset{\sim}{\Delta} \end{cases} \quad (21)$$

$$\begin{aligned} U_k = -(GaB)^{-1}[&-\Delta s_k + GaA\Delta e_k + Gad_{k-1} \\ &+k_I\Delta\xi_k + Ga\left(k_m sign\left(\Delta s\right) + \eta\Delta s\right)] \end{aligned} \quad (22)$$

From equations (22), (20) and (16), the subsequent series of the sliding segment can be created as

$$\begin{aligned} \Delta s_{k+1} &= Ga\Delta e_{k+1} + k_I\Delta\xi_k \\ &= Ga\left(A\Delta e_k + BUc_k + d_k\right) + k_I\Delta\xi_k \\ &= \Delta s_k + Ga\underset{\sim k}{\varepsilon} - Ga\left(k_m sign\left(\Delta s\right) + \eta\Delta s\right) \end{aligned} \quad (23)$$

$\underset{\sim k}{\varepsilon} = d_k - d_{k-1}$ is a vector of error assessed for the disturbance, and it is assumed to be limited as

$$\left|\underset{\sim k}{\varepsilon}\right| = d_k - d_{k-1} \le \Delta_d \quad (24)$$

Assume the switching regulation coefficient vector $K_{s\sigma}$ is set to meet the following case

$$|K_{s\sigma}| > \Delta_d + \sigma \quad (25)$$

where σ is a (+) fixed arbitrary scalar. And in the condition of $\Delta s_k \geqslant 0$,

$$\begin{aligned} \Delta s_{k+1} &= \Delta s_k - GaK_{s\sigma} + Ga\varepsilon_k \\ &< \Delta s_k - Ga[\Delta_d + \sigma - \varepsilon_k] \\ &< \Delta s_k \end{aligned} \quad (26)$$

Furthermore, when $\Delta s_k \leqslant 0$, the following can be deduced

$$\begin{aligned} \Delta s_{k+1} &= \Delta s_k - GaK_{s\sigma} + Ga\varepsilon_k \\ &> \Delta s_k + Ga[\Delta_d + \sigma + \varepsilon_k] \\ &> \Delta s_k \end{aligned} \quad (27)$$

substitute (26)into (27)

$$|\Delta s_{k+1}| < \Delta s_k \ for\ k \geqslant k_0 \tag{28}$$

Thus, the $|\Delta s_{k+1}|$ shows that the step-ahead sliding sequences are decreased routinely, and the discrete-time sliding variable is moving on the desired sliding plane after a limited number of stages k_0. It has been indicated in (Sarpturk et al., 1987) that the relationship (28) introduces an essential condition for the existence of discrete-time sliding mode. Theorem-1: gives an essential condition for the existence of the discrete-sequences sliding mode. Due to the disconnected signum term, $sgn(s)$, chattering may appear in the regulator input. As mentioned, to reduce the chattering state, the suppress layer method is selected by substituting the signum term in (22) with the saturation term.

$$sat(\Delta(s_k)) = = \begin{cases} sgn(s_k), \text{If} |s| > \underset{\sim}{\Delta} \\ ks_k, \quad \text{If} |s| \leq \underset{\sim}{\Delta}, k = 1/\underset{\sim}{\Delta} \end{cases} \tag{29}$$

where the positive scalar factor $\underset{\sim}{\Delta}$ denotes the suppress layer range, which keeps that s_k is consistently limited by $\pm\underset{\sim}{\Delta}$. The factor selection is carried out by exchanges between the chattering and searching deviation. Equation (25) presents that the control coefficient selection $K_{s\sigma}$ depends on the upper limit of the evaluated disturbance deviation Δ_d. In standard SMC, the upper limit of the disturbance is a substitute in this term. Generally, the evaluated disturbance deviation is much low compared to the disturbance signal. Hence, the coefficient vector with lower switching can be designed compared to the standard SMC. This feature enhances the PSMC during the one-step shift of the evaluated disturbance over the standard SMC.

2.4 RPSMC-PSO Controller Design

The RPSMC-PSO module is created to regulate the particular dynamic states that appear on the system. In particular, the PSO based on neural network produces optimal sequences of the sliding surface to determine the ideal control law solutions U_k^{pso}, and the identical control Uc_k is employed to accurate the state path of the sliding switches along with the future sampling time without chattering conduct. Hence, the total control law is

$$Ue_k = Uc_k + U_k^{pso} \tag{30}$$

From equations (30) and (16), yields

$$\begin{aligned} \Delta s_{k+1} &= Ga\Delta e_{k+1} + k_I \Delta \xi_k \\ &= Ga\left(A\Delta e_k + BUe_k + d_k\right) + k_I \Delta \xi_k \\ &= Ga\left(A\Delta e_k + B\left(Uc_k + U_k^{pso}\right) + d_k\right) + k_I \Delta \xi_k \\ &= \Delta s_k + GaBU_k^{pso} + Ga\underset{\sim k}{\varepsilon} \end{aligned} \tag{31}$$

According to (31), the sliding path is defined in compact form as

$$\begin{aligned} \Delta s_{k+1} &= \Omega \Delta s_k + \Phi \Delta u_k + \Gamma \underset{\sim k}{\varepsilon} \\ \bar{y}_k &= H\Delta s_k \end{aligned} \tag{32}$$

In (32), the parameter matrices are specified as $\Omega = [I]$, $\Phi = [GaB]$ and $\Gamma = [Ga]$. A standard augmented formula (33) can be assembled based on the sliding function state space in (32). The dimensions of matrices are defined as $m = 2$, $n = 2$ *and* $q = 2$. $x_h(k) = [\Delta s(k)\ \bar{y}(k)]^T$ is a vector that is defined by a new structure of variables (Liu and Kong, 2013).

$$\begin{aligned} \overbrace{\begin{bmatrix} \Delta s(k+1) \\ \bar{y}(k+1) \end{bmatrix}}^{x_h(k+1)} &= \overbrace{\begin{bmatrix} \Omega_{m\times m} & 0_{m\times q} \\ H\Omega_{q\times m} & I_{q\times q} \end{bmatrix}}^{A_h} \overbrace{\begin{bmatrix} \Delta s(k) \\ \bar{y}(k) \end{bmatrix}}^{x_h(k)} + \overbrace{\begin{bmatrix} \Phi_{m\times n} \\ H\Phi_{q\times n} \end{bmatrix}}^{B_h} \Delta u(k) \\ &\quad + \overbrace{\begin{bmatrix} \Gamma_{m\times n} \\ \Phi\Gamma_{q\times n} \end{bmatrix}}^{E_h} \underset{\sim}{\varepsilon}(k) \\ \bar{y}(k) &= \overbrace{[0_{q\times m}\ I_{q\times q}]}^{C_h} \begin{bmatrix} \Delta s(k) \\ \bar{y}(k) \end{bmatrix} \end{aligned} \tag{33}$$

The augmented formula identifies the SMC's dynamic features, besides determining a single-stage of best prediction sliding switch path. Thus, the best-predicted solution of the sliding population elements (pe) can be generated using the PSO algorithm based on (33) at each iteration (it):

$$\begin{aligned} y_{(k+\{pe,it\}|k)} = \bar{E}x_{(k+\{pe,it\}|k)} + \bar{N}\Delta u_{(k+\{pe,it\}|k)} + \\ \bar{\Lambda}\underset{\sim(k+\{pe,it\}|k)}{\varepsilon} \end{aligned} \tag{34}$$

where $\bar{E} = [C_h A_h]_{pe}$, $\bar{N} = [C_h B_h]_{pe}$ and $\bar{\Lambda} = [C_h E_h]_{pe}$. The PSO algorithm based on (34) makes the cost function formula to be minimized as follows (Shi et al., 2019). The PSO algorithm focuses on identifying the ideal control law solutions of SMC besides the identical control law to ensure the accuracy of the state path of the sliding switches along with the future sampling time without high chattering in the non-linear DFIG-WT variables in respect of optimization problem, which aims for reducing the cost-function defined as the sum of squared error of sliding states based on rotor-aspect current and the predicted control signal sequences based on PSO algorithm.

$$\begin{aligned} J(\Delta u_k) &= \left| y_{k+1}^{ref} - y_{k+1} \right|_{\phi_y}^2 + |u_k - u_{k-1}|_{\lambda_u}^2 \\ \text{s.t}\ \ \Delta u_{\min} &\leq \Delta u(k) \leq \Delta u_{\max},\ y_{\min} \leq y(k) \leq y_{\max} \end{aligned} \tag{35}$$

where y^{ref} is the desired signal, ϕ_y and λ_u are the matrices including positive elements. Therefore, the final minimization step of (35) involving the formula (34) is obtained as

$$u_k = u_{k-1} + \frac{\rho_k \bar{N}^T \phi_y}{\bar{N}^T \phi_y \bar{N} + \lambda_u}(y_{k+1}^* - y_k) \tag{36}$$

ρ_k is the output sequence step distance.

3. PSO-ALGORITHM BASED RPSMC CONTROLLER

3.1 General Concept of PSO Optimization

PSO Algorithm is a randomized directive algorithm has been designed by Eberhart and Russel (2015). This algorithm searches for the best choice among the population of swarm solutions. Thus, randomly N particles are produced in the searching range (Zapata et al., 2020). In discrete-time model, an individual particle i and its position and velocity are defined as x_i^k and v_i^k at each sampling interval k respectively. The two variables U^{pso} are defined as the algorithm's problem, and the particle position x_i^k and velocity v_i^k are set to be the solution and its limited variance

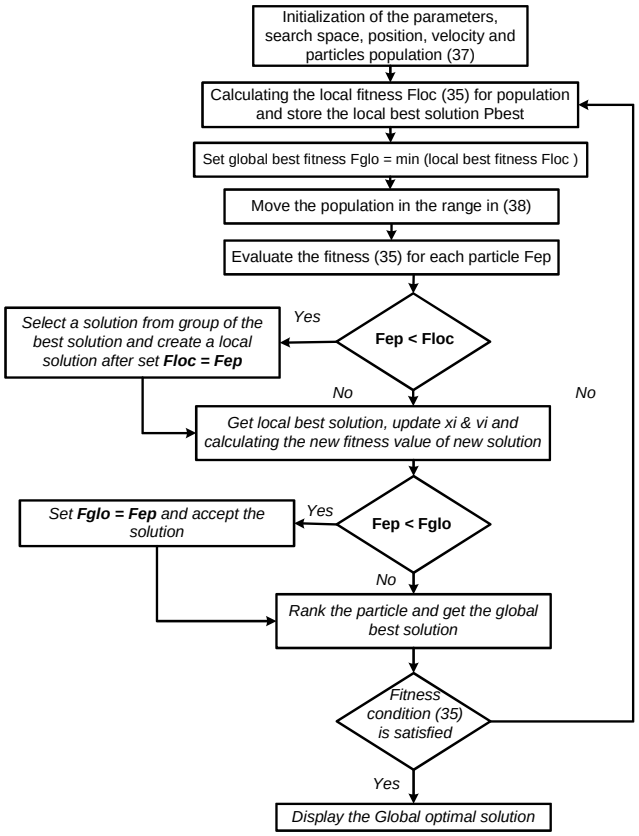

Fig. 9. Flow-chart of PSO Algorithm code.

by v_{min} and v_{max} value through solution space respectively. The solution or optimal position of each particle is preserved in P_{best} at each sample time G_{best} is defined as the position that contains the registered best performance of individuals along with the population at each sample time k. This idea offers a weighted incompatible acceleration during the movement at the iterations range. Then, the initial position is evaluated along with the specified population.

$$x_{ij} = x_{\min} + rand(x_{\max} - x_{\min}) \tag{37}$$

where $i = 1, 2, \ldots, N, j = 1, \ldots, d$ and x_{max}/x_{min} are the limited values for population, and $rand \in (0, 1)$. Adaptation of the particle's position is influenced by the rates of fitness law (35). In general, a new position x_i^{k+1} is evaluated within the searching space.

$$\begin{aligned} v_i^k &= \omega v_i^{k-1} + c_1 \text{rand}[0,1](P_{best} - x_i^{k-1}) \\ &\quad + c_2 \text{rand}[0,1](G_{best} - x_i^{k-1}) \\ x_i^k &= x_i^{k-1} + v_i^k \end{aligned} \tag{38}$$

where ω is the decreased unity element at each iteration, $c_1 = c_2 = 3$ are the positive number. rand $\in (0, 1)$ is a random amount. Figs. 9 and 10 display the flow-chart of standard PSO-Algorithm and the convergence of MSE during effective iterations for the PSO-algorithm included in the RPSMC approach. According to the 30 swarm searching range, the first active iterations time of the PSO during the fixed rotor aspect speed case is 24.508 sec.

3.2 RPSMC based on PSO Optimization

PSO-Algorithm based RPSMC approach procedures are defined as following steps

- **Step-1:**. Initialize:
  - **A-** According to the model in Fig. 4, Two variables items U^{pso} of RPSMC-PSO needs to be optimized. Thus, the variable dimension is set as $d = 2$.
  - **B-** The system parameters are defined related to the DFIG-WTs nominal values as in Table 1, the algorithm parameters are $\omega = 0.6$, $c_1 = c_1 = 2$, searching (population) range is defined as ($N = 30$), restriction values are [2,-1], Max-iteration space is $Itr_{max} = 30$, and the tolerance is $10e^{-5}$. (All these parameters are chosen by User).
  - **C-** population are randomly selected to define the particles position x_i and velocity v_i;
  - **D-** Inspect whether each particle values are feasible status, i.e. meet the mechanism restrictions;
- **Step-2:**. Compute the evaluated fitness value based on the sum of squared error of sliding states based on rotor-aspect current and the predicted control signal sequences for each particle items P_{ai} by using the cost function (35): The optimal solution guarantees the best tracking path between the system output and input by generating best control action $u(k)$.
- **Step-3:** Initialize each (P_{best}) to match the present position of the separated particles P_{ai}.
- **Step-4:**. **While** ($N_l < Iter_{max}$);
- **Step-5:**. Compare each fitness amount of P_{ai} with basic P_{best}, and put the global amount as G_{best} as the best amount for all P_{best}.
- **Step-6:**. Produce new velocity amount of P_{ai} step using (38).
- **Step-7:**. Ensure the velocity amount not exceed the restriction values.
- **Step-8:**. Generate a new position of each P_{ai} using (37) and (35) in **Step-2:**.
- **Step-9:**. Inspect whether each new P_{ai} is a feasible status. And adjust the P_{best} as the current x_i^{k+1}, when its evaluated fitness amount of the advanced particle x_i^{k+1} is better than past P_{best} (k-1). Thus, G_{best} is replaced by P_{best}, when the P_{best} amount is better than G_{best}.
- **Step-10:**. **If condition:** ($N_l = Iter_{max}$, then select last G_{best}) (a new G_{best} amount is found); and go to **Step-11**; **Else**, go to **Step-2**. **End**.
- **Step-11:**. The particle P_{ai} that generated the latest G_{best} indicates the scheduled optimal control factors at each effective sample time.
- Finally, the optimal amounts of u are applied to produce the overall RPSMC signals.

4. ANALYSIS OF THE RESULTS

Figs. 11- 12, demonstrate the general connections of the DFIG-WT and the schematic of the RPSMC, which including the PSO strategy, which simulated using Matlab-toolbox. As observed, the DFIG stator-aspect is directly attached to the power source network, while the DFIG rotor-aspect under-regulated is linked to the IGBT bi-way converter. A high-frequency filter is tied with the stator-

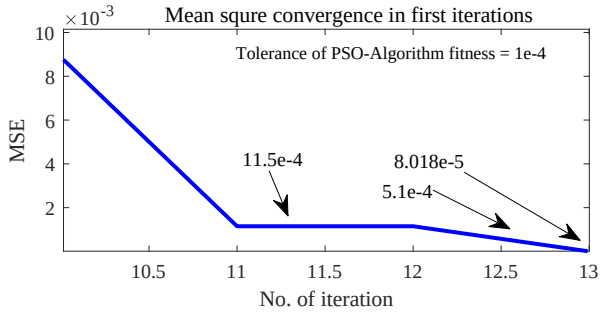

Fig. 10. MSE Convergence of PSO algorithm during effective iterations.

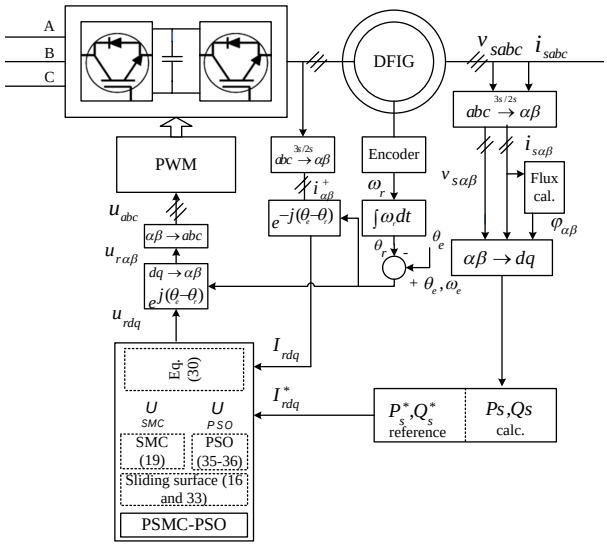

Fig. 11. Diagram of the RPSMC technique for the DFIG.

element to constrict the harmonics stirred by converters (Zhi and Xu, 2007). The DFIG coefficients and the evaluated dynamic quantities are shown in Table 1. Dynamic comparisons of the conventional SMC and PI controllers have been utilized to affirm the dynamic contrast in the performance of the proposed RPSMC-PSO strategy. The parameters of the conventional SMC and PI controllers are adapted using off-line adaptation by using PSO algorithm. where ($KP_p = 0.0056$, $KP_i = 0.4938$) and ($KQ_p = 5.7e-3$, $KQ_i = 4.938$), and ($C_d = 3.5$, $C_i = 3.5$, $K_M = 360$ and $miu = 0.8$) are the parameters values of the conventional PI and SMC regulator. Furthermore, the comparison study incorporates four cases, the DFIG under the fixed, sub-, and super-synchronous situation contingent upon the different swings of the rotor speed, a perturbation in the rotor flux, and grid unbalanced situation.

At first, the dynamic conduct of the DFIG-WT in light of the proposed RPSMC-PSO strategy is investigated for different reference steps of stator-aspect power Ps and Qs.

Table 1. Rated coefficients of the DFIG-WT

Nominal Parameters			
Power	1.5 MW	Stator Voltage	563V
Rs/Rr	2.6/2.9 mΩ	*Vdc*	1150 V
Ls/Lr/Lm	2.6/2.6/2.5 mH	Freq.	50Hz
No. pole	4	M. inertia J	$26Km^2$

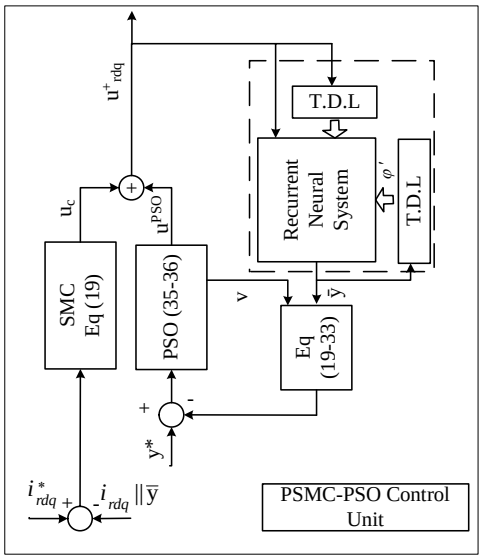

Fig. 12. The internal links of the RPSMC control unit.

As appeared in Figs. 13(f and e), the desired Ps is set from 0.35 to 0.75 pu at 0.5 sec, and after 0.25 sec is passed, the desired Ps is set to 1 pu meanwhile, the desired Qs power is fixed at 0 pu. The first investigation has been fulfilled with a fixed rotor velocity at 1630 rev/min (1.086 pu). Generally, the estimated RPSMC-PSO controller of the DFIG is composed of SMC part based on linear features of a low degree Taylor approximation series for RNN to build the optimal sliding switches. As shown in Fig. 13(f), the

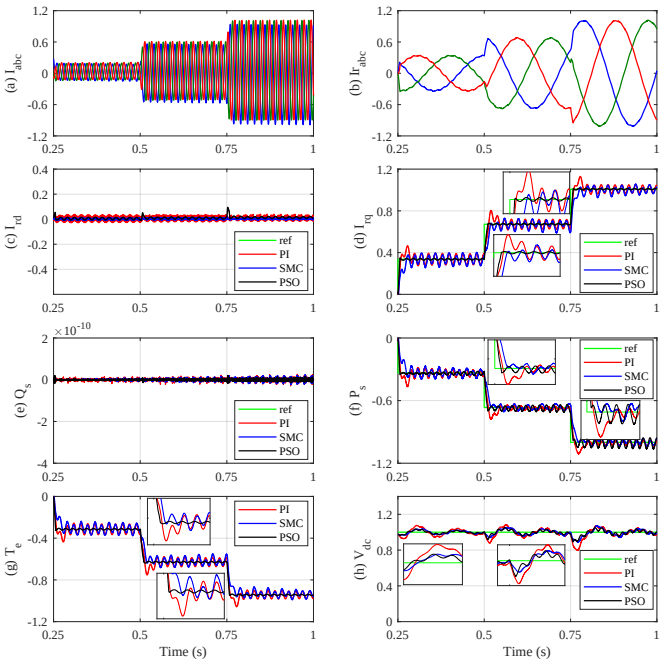

Fig. 13. The DFIG-WT responses based on RPSMC-PSO (black), SMC (green) and PI (red) during normal operation status (a) AC stator-aspect current based on proposed control. (b) AC rotor-aspect current based on proposed control. (c) *d*-axis of the rotor-aspect current. (d) *q*-axis of the rotor-aspect current. (e) Qs step response. (f) Ps step response. (g) electromagnetic torque response. (h) DC-link voltage response.

RPSMC-PSO carried out superior dynamic action than PI and traditional SMC strategy due to the low overshoot and fast reaction over the power reference stages. The overshoot percentage amount attributed to Ps is (6.32%, 13.4%, 39%) at 0.25 sec, (3.91%, 5.5%, 16.9%) at 0.5 sec and (4.90%, 4.2%, 10.9%) at 0.75 sec for the offered controller, SMC and PI, respectively. And its rise time is (5.91, 8.2, 24.7 msec) at 0.25 sec, (9.32, 52, 12.1 msec) at 0.5 sec and (14.81, 54.1, 11.6 msec) at 0.75 sec for the RPSMC-PSO, SMC and PI, respectively. The settling time attributed to Ps is (12.22, 45, 36.6 msec) at 0.25 sec, (25.31, 80, 64.1 msec) at 0.5 sec and (46.32, 70, 58.1 msec) at 0.75 sec for the RPSMC-PSO, SMC and PI, respectively. As viewed in Fig. 13(d), the RPSMC-PSO accomplished good follow of the performance at dq-reference frame for the rotor-aspect current with smaller overshot, current vibration ripple, and fast reaction for corresponding steps of Ps than PI and SMC controller. where the i^{rq} overshoot percentage amount is (5.1%, 12.6%, 38%) at 0.25 sec, (1.32%, 1.9%, 20%) at 0.5 sec and (1.6%, 2.8%, 12.8%) at 0.75 sec for the offered controller, SMC and PI, respectively. And its rise time is (6.11, 8.3, 25 msec) at 0.25 sec, (10.21, 17.7, 13.2 msec) at 0.5 sec and (7.33, 26.3, 9.8 msec) at 0.75 sec for the RPSMC-PSO, SMC and PI, respectively. And the settling time is (10.1, 46, 36 msec) at 0.25 sec, (18.81, 36.5, 46.1 msec) at 0.5 sec and (13.92, 45.7, 38.3 msec) at 0.75 sec for the RPSMC-PSO, SMC and PI, respectively. Fig. 13(a) and (b), can appear that the RPSMC-PSO strategy set the frequency of the stator-/rotor-aspect current is stable sequences during the power steps protruded.

In Fig. 13 (g and h), the torque and DC voltage signal under RPSMC-PSO, traditional SMC and PI give a vast overshoot close to (6.42%, 4%, 1.6%), (12.91%, 4.6%, 2.1%) and (39.73%, 22.9%, 12.4%) at 0.25, 0.5 and 0.75 sec, and (19.3%), (26.5%) and (33.6%), respectively. And rise time of RPSMC-PSO, SMC and PI are (6.33, 9.8, 7 msec), (25.71, 17.4, 26.5 msec) and (8.72, 13.7, 10 msec) at 0.25, 0.5 and 0.75 sec, and (8.05 msec) for all controllers, respectively. And settling time of RPSMC-PSO, SMC and PI are (14.14, 17, 12.9 msec), (46.61, 36.2, 46.3 msec) and (36.23, 45, 38.2 msec) at 0.25, 0.5 and 0.75 sec, and 0.113, 0.140 and 0.152 sec, respectively.

In Fig. 14, the varied desired stator-aspect active power input is formed as pulsing and ascending and descent stair signals. The RPSMC-PSO introduced a higher tracking behavior and fast response close to the dynamic reaction of the BATS-SMC at each new stage with oscillations compared to common SMC and PI regulators.

In the fact-time application of WT, a wind wave velocity changes inherently. The turbine's speed control may not deliver a fast response to recover the sharp change in the four operating modes, influencing the efficiency or deteriorating the system appliances. The advanced wind generation model based on the DFIG comprises the slip correlation method to save the electrical variables frequency suitable to the common network frequency while the wind speed exchange. The RPSMC-PSO strategy is achieved with an incline of the rotor angular speed from 1630 to 1300 rev/min (1.09 pu super-synchronous to 0.87 pu sub-synchronous mode) at the time-space 0.4-0.6 sec then it climbs back to the first point from 0.8 sec, as

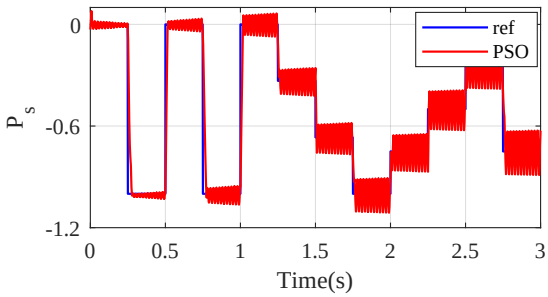

Fig. 14. Ps step response related to the varied desired input.

demonstrated in Fig. 15 (c). Whereas the Ps is altered from -1 to -0.35 pu between 0.55 and 0.95 sec, meanwhile, the ripples are increased in Qs as in Figs. 15(a-b).

As appeared in Figs. 15(g) and (f), the i_{rq} and i_{rd} were altered from 1 to 0.36 pu and 0 to -0.5 between 0.55 and 0.95 sec, respectively. Also in Figs. 15(h) and (i), the mechanical torque was altered from -1 to -0.38 pu and the DC-link controller maintains constant voltage stability. As appeared in Figs. 15(e), the RPSMC-PSO modified the rotor-aspect phases to maintain its signal sequences. In Figs. 15, the RPSMC-PSO has a preference with a good follow the performance at dq-reference form of rotor current, with the smallest overshoot, less vibration ripple, and fast reaction along the period of the reference signal.

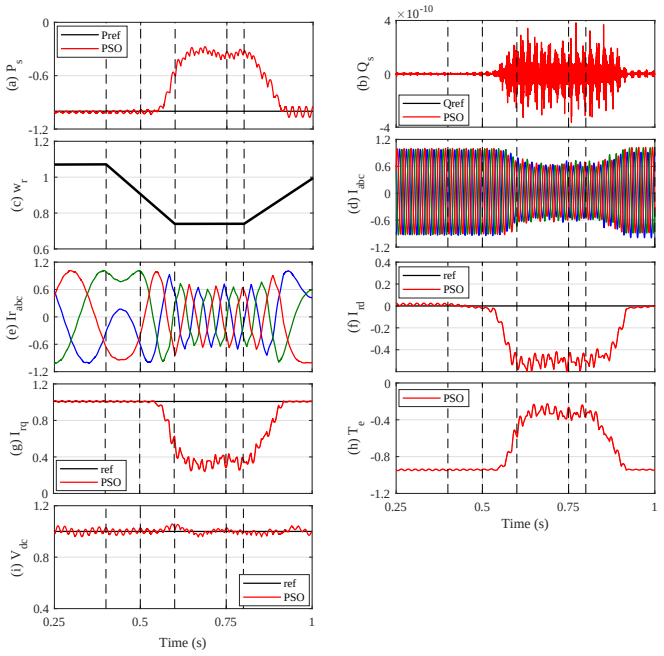

Fig. 15. The DFIG-WT responses based on RPSMC-PSO during change in rotor speed (a) Ps step response. (b) Qs step response. (c) rotor speed curve. (d) AC stator-aspect current. (e) AC rotor-aspect current. (f) q-axis of rotor-aspect current. (g) d-axis of rotor-aspect current. (h) electromagnetic torque response. (i) DC-link voltage response.

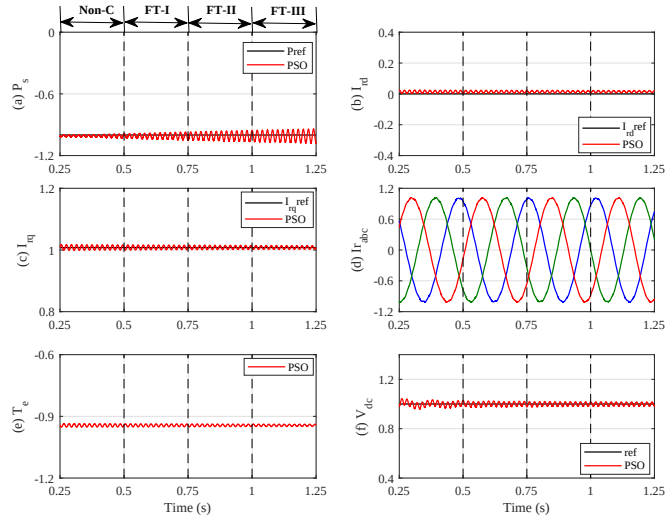

Fig. 16. The DFIG-WT responses based on RPSMC-PSO during change in rotor speed (a) Ps step response. (b) Qs step response. (c) *d*-axis of rotor-aspect current. (d) *q*-axis of rotor-aspect current. (e) AC stator-aspect current. (f) AC rotor-aspect current. (g) electromagnetic torque response. (h) DC-link voltage response.

The fact-time control system is vulnerable to assorted surrounding influences on the system characteristics. In Fig. 16, to clarify the parameters variations comparisons, the dynamic inspection is attained assuming that the resistors of the stator/rotor and the combined inductor are reduced by -50% in Case-I. Moreover, $+50\%$ and -50% are included in resistors and combined inductors in case-II, respectively. Besides, the values were extended to $+50\%$ for overall parameters in case-III along with the reference signals. The simulation results in Fig. 16 demonstrate that the dynamic achievement of the DFIG-WT based upon the proposed strategy raised the robustness of the RPSMC-PSO with the smallest overshoot, less current vibration ripple and fast reaction for all stages during parameter variations. There is no significant change in the response form, with ascendant ripples in the power signal over case-I,II, and case-III as in Fig. 16 (a). This part provides an additional study on the suggested RPSMC-PSO strategy, and the generation system has been investigated during

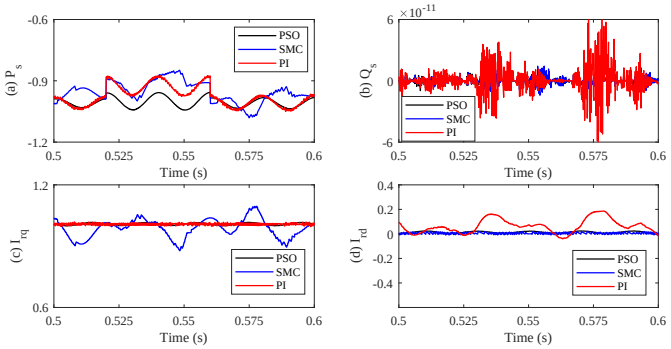

Fig. 17. The DFIG-WT responses based on RPSMC-PSO during unbalanced-voltage status (a) Ps step response. (b) Qs step response. (c) *d*-axis of rotor-aspect current. (d) *q*-axis of rotor-aspect current.

an unbalanced voltage case. In fact-time, there are various factors to occur these kinds of disturbances such as unstable distribution, external faults, load, etc. In this test, the system is running at a super-synchronous condition (1.086 p.u, 1630r/min) which is identical to a $+8.66\%$ slip amount, while the desired stator-aspect active power is adjusted to maximum amounts 1 p.u (1.5 MV). The AC fault was set at 0.5-0.6 sec, limiting the stator voltage to 0.9 pu of the named value.

Figs. 17(a-d) shows the fault affection of the supply voltage on the stator-aspect power and rotor-aspect current, respectively, and the comparison implemented between RPSMC-PSO, SMC, and PI controller. The stator-aspect power and *dq* rotor-aspect current are manipulated during the fault condition. The oscillations of stator-aspect power and rotor-aspect current that resulted from RPSMC-PSO have lower ripples than the PI controller.

The overall system that included the non-linear DFIG restrained the stator-aspect power and current and regulated the rotor voltage within the nominated range by noting the results given during unbalanced grid-tied conditions. Generally, the RPSMC-PSO based DFIG-WT system generates a proper implementation for both balanced and unbalanced grid-linked conditions.

5. CONCLUSION

This article has exhibited the rotor-aspect current control based on stator-aspect power using an optimal sliding mode control approach RPSMC-PSO based on a linear Taylor approximation formula of the non-linear DFIG-WT based on RNN. RPSMC-PSO construction included the PSO algorithm based on a neural network controller RNN, which uses the MIMO variables of the system to detect optimum sliding chattering trajectories. The suggested mechanism and traditional control applied for the rotor, and grid-aspect bi-way IGBT converters handle the rotor-aspect current and stator-aspect power signals to trace the coveted inputs. Thus, RPSMC-PSO delivered the *dq*-axis rotor voltage as control signals to the rotor-aspect converter. The simulation events for a 1.5MW DFIG-WT have been rendered and compared with two kinds of traditional control, PI and SMC strategies. The dynamic execution of the RPSMC-PSO strategy has been achieved with various running cases (sub- and super-synchronous cases) based on the rotor-speed alteration. Additional enhancement test has been accomplished to compare the proposed strategy through uncertainty parameters and unbalanced-voltage on the power network. The simulated dynamic results validated that the RPSMC-PSO has been performed good tracking, less overshoot, and low oscillation of electrical amounts than traditional control units. RPSMC-PSO regulated the WT system successfully for running during interchange within two angular speed modes and abnormal-running conditions.

REFERENCES

Akpan, V. and Hassapis, G. (2011). Nonlinear model identification and adaptive model predictive control using neural networks. *ISA transactions*, 50(2), 177–194.

Alzain, O.B., Liu, X., Kong, X., Alzain, A.B., Abdalla, M.A., and Ali, D.A. (2019). Improved DFIG-WPGS efficiency via the tuned PI-resonant unit controller based on BAT algorithm. In *2019 International Conference on Computer, Control, Electrical, and Electronics Engineering (ICCCEEE)*, 1–7. IEEE.

Alzain, O.B., Liu, X., and Ali, A. (2021). Optimization of SMC-R control based rotor current using Bird Swarm algorithm for the distorted DFIG-WPS. In *2020 International Conference on Computer, Control, Electrical, and Electronics Engineering (ICCCEEE)*, 1–7. IEEE.

Balduzzi, D., McWilliams, B., and Butler-Yeoman, T. (2017). Neural Taylor approximations: Convergence and exploration in rectifier networks. In *International Conference on Machine Learning*, 351–360. PMLR.

Beltran, B., Ali, T., and Benbouzid, M. (2008). High-order sliding-mode control of variable-speed wind turbines. *IEEE Transactions on Industrial electronics*, 56(9), 3314–3321.

Chen, S., Cheung, Wong, K., and Wu, J. (2009). Integral sliding-mode direct torque control of doubly-fed induction generators under unbalanced grid voltage. *IEEE transactions on energy conversion*, 25(2), 356–368.

Cheng, C. and Nian, H. (2017). Low-complexity model predictive stator current control of DFIG under harmonic grid voltages. *IEEE Transactions on Energy Conversion*, 32(3), 1072–1080.

Costa, J., Pinheiro, H., Degner, T., and Arnold, G. (2010). Robust controller for DFIGs of grid-connected wind turbines. *IEEE transactions on industrial electronics*, 58(9), 4023–4038.

Du, H., Yu, X., Chen, M., and Li, S. (2016). Chattering-free discrete-time sliding mode control. *Automatica*, 68, 87–91.

Ganti, V., Singh, B., Aggarwal, S., and Kandpal, T. (2011). DFIG-based wind power conversion with grid power leveling for reduced gusts. *IEEE Transactions on Sustainable Energy*, 3(1), 12–20.

Guo, Z., Wang, J., and Yan, Z. (2014). Global exponential synchronization of two Memristor-based recurrent neural networks with time delays via static or dynamic coupling. *IEEE Transactions on Systems, Man, and Cybernetics: Systems*, 45(2), 235–249.

Hu, J., Nian, H., Hu, B., He, Y., and Zhu, Z. (2010a). Direct active and reactive power regulation of dfig using sliding-mode control approach. *IEEE Transactions on energy conversion*, 25(4), 1028–1039.

Hu, J., Nian, H., Xu, H., and He, Y. (2010b). Dynamic modeling and improved control of DFIG under distorted grid voltage conditions. *IEEE transactions on energy conversion*, 26(1), 163–175.

Jabr, H., Lu, D., and Kar, N. (2011). Design and implementation of Neuro-Fuzzy vector control for wind-driven doubly-fed induction generator. *IEEE Transactions on Sustainable Energy*, 2(4), 404–413.

Liu, X. and Kong, X. (2013). Nonlinear model predictive control for DFIG-based wind power generation. *IEEE Transactions on Automation Science and Engineering*, 11(4), 1046–1055.

Martinez, M., Susperregui, A., Tapia, G., and Xu, L. (2013). Sliding-mode control of a wind turbine-driven double-fed induction generator under non-ideal grid voltages. *IET Renewable Power Generation*, 7(4), 370–379.

Martinez, M., Tapia, G., Susperregui, A., and Camblong, H. (2012). Sliding-mode control for DFIG rotor-and grid-side converters under unbalanced and harmonically distorted grid voltage. *IEEE Transactions on Energy Conversion*, 27(2), 328–339.

Nazari, Alireza, and Heydari, H. (2011). Enhanced predictive direct power control of DFIG. In *2011 2nd Power Electronics, Drive Systems and Technologies Conference*, 15–19.

Omar, B., Liu, X., and Ali, A. (2021). Optimization of sliding mode control based on BAT-algorithm for the DFIG-WT. In *2020 International Conference on Computer, Control, Electrical, and Electronics Engineering (ICCCEEE)*, 1–7. IEEE.

Pan, Y. and Wang, J. (2011). Model predictive control of unknown nonlinear dynamical systems based on recurrent neural networks. *IEEE Transactions on Industrial Electronics*, 59(8), 3089–3101.

Pande, V., Mate, U., and Kurode, S. (2013). Discrete sliding mode control strategy for direct real and reactive power regulation of wind driven DFIG. *Electric Power Systems Research*, 100, 73–81.

Patnaik, R. and Dash, P. (2016). Fast adaptive back-stepping terminal sliding mode power control for both the rotor-side as well as grid-side converter of the doubly fed induction generator-based wind farms. *IET Renewable Power Generation*, 10(5), 598–610.

Precup, R.E., David, R.C., Roman, R.C., Petriu, E.M., and Szedlak-Stinean, A.I. (2021). Slime Mould Algorithm-based tuning of cost-effective Fuzzy controllers for servo systems. *International Journal of Computational Intelligence Systems*, 14(1), 1042–1052.

Qiao, W., Qu, L., and Harley, R. (2009). Control of IPM synchronous generator for maximum wind power generation considering magnetic saturation. *IEEE Transactions on Industry Applications*, 45, 1095–1105.

Qin, S. and Badgwell, T. (2003). A survey of industrial model predictive control technology. *Control engineering practice*, 11(7), 733–764.

Rekioua, D. (2014). Optimisation of wind system conversion. In *Wind Power Electric Systems*, 77–105. Springer.

Repta, D., Dumitrache, I., Sacala, I.S., Moisescu, M.A., Stanescu, A.M., and Caramihai, S.I. (2018). Automated process recognition architecture for Cyber-Physical systems. *Enterprise Information Systems*, 12(8-9), 1129–1148.

Ruiz-Cruz, R., Sanchez, E., Ornelas-Tellez, F., Loukianov, A., and Harley, R. (2012). Particle Swarm Optimization for discrete-time inverse optimal control of a doubly fed induction generator. *IEEE transactions on cybernetics*, 43(6), 1698–1709.

Sarpturk, S., Istefanopulos, Y., and Kaynak, O. (1987). On the stability of discrete-time sliding mode control systems. *IEEE Transactions on Automatic Control*, 32(10), 930–932.

Shang, L. and Hu, J. (2012). Sliding-mode-based direct power control of grid-connected wind-turbine-driven doubly fed induction generators under unbalanced grid voltage conditions. *IEEE Transactions on Energy Conversion*, 27(2), 362–373.

Shi, K., Yin, X., Jiang, L., Liu, Y., Hu, Y., and Wen, H. (2019). Perturbation estimation based nonlinear adap-

tive power decoupling control for DFIG wind turbine. *IEEE Transactions on Power Electronics*, 35(1), 319–333.

Su, X., Liu, X., Shi, P., and Yang, R. (2016). Sliding mode control of discrete-time switched systems with repeated scalar nonlinearities. *IEEE Transactions on Automatic Control*, 62(9), 4604–4610.

Sun, D. and Wang, X. (2017). Sliding-mode DPC using sogi for DFIG under unbalanced grid condition. *Electronics Letters*, 53(10), 674–676.

Sun, D., Wang, X., Nian, H., and Zhu, Z. (2017). A sliding-mode direct power control strategy for DFIG under both balanced and unbalanced grid conditions using extended active power. *IEEE Transactions on Power Electronics*, 33(2), 1313–1322.

Valenciaga, F. and Puleston, P. (2008). High-order sliding control for a wind energy conversion system based on a permanent magnet synchronous generator. *IEEE Transactions on Energy Conversion*, 23, 860–867.

Wang, T., Gao, H., and Qiu, J. (2015). A combined adaptive neural network and nonlinear model predictive control for multirate networked industrial process control. *IEEE Transactions on Neural Networks and Learning Systems*, 27(2), 416–425.

Xiang, K., Li, B., Zhang, L., Pang, M., Wang, M., and Li, X. (2016). Regularized Taylor Echo state networks for predictive control of partially observed systems. *IEEE Access*, 4, 3300–3309.

Xu, H., Hu, J., and He, Y. (2012). Integrated modeling and enhanced control of DFIG under unbalanced and distorted grid voltage conditions. *IEEE Transactions on Energy Conversion*, 27(3), 725–736.

Xu, Q. and Li, Y. (2011). Model predictive discrete-time sliding mode control of a nanopositioning piezostage without modeling hysteresis. *IEEE Transactions on Control Systems Technology*, 20(4), 983–994.

Yan, Z. and Wang, J. (2012). Model predictive control of nonlinear systems with unmodeled dynamics based on Feedforward and Recurrent neural networks. *IEEE Transactions on Industrial Informatics*, 8(4), 746–756.

Yılmaz, S. and Küçüksille, E. (2015). A new modification approach on BAT algorithm for solving optimization problems. *Applied Soft Computing*, 28, 259–275.

Young, K., Utkin, V., and Ozguner, U. (1999). A control engineer's guide to sliding mode control. *IEEE transactions on control systems technology*, 7(3), 328–342.

Yu, D. and Gomm, J. (2003). Implementation of neural network predictive control to a multivariable chemical reactor. *Control Engineering Practice*, 11(11), 1315–1323.

Yu, S. and Long, X. (2015). Finite-time consensus for second-order Multi-Agent systems with disturbances by Integral sliding mode. *Automatica*, 54, 158–165.

Zamarreño, M.J. and Vega, P. (1998). State space neural network. properties and application. *Neural networks*, 11(6), 1099–1112.

Zapata, H., Perozo, N., Angulo, W., and Contreras, J. (2020). A hybrid Swarm Algorithm for collective construction of 3d structures. *Int. J. Artif. Intell*, 18(1), 1–18.

Zeddini, M., Pusca, R., Sakly, A., and Mimouni, M. (2016). Pso-based MPPT control of wind-driven self-excited induction generator for pumping system. *Renewable Energy*, 95, 162–177.

Zemouri, R., Gouriveau, R., and Zerhouni, N. (2010). Defining and applying prediction performance metrics on a recurrent NARX Time series model. *Neurocomputing*, 73(13-15), 2506–2521.

Zhang, X. and Hou, B. (2017). Double vectors model predictive torque control without weighting factor based on voltage tracking error. *IEEE Transactions on Power Electronics*, 33(3), 2368–2380.

Zhi, D. and Xu, L. (2007). Direct power control of DFIG with constant switching frequency and improved transient performance. *IEEE Transactions on Energy Conversion*, 22(1), 110–118.

Zhou, Y., Bauer, P., Ferreira, J., and Pierik, L. (2009). Operation of grid-connected DFIG under unbalanced grid voltage condition. *IEEE Transactions on Energy Conversion*, 24(1), 240–246.